Exceptional electromagnetic interference shielding and microwave absorption properties of room temperature synthesized polythiophene thin films with double negative characteristics (DNG) in the Ku-band region

Gopal Kulkarni, Priyanka Kandesar, Ninad Velhal, Varsha Phadtare, Aviraj Jatratkar, S.K. Shinde, Dae-Young Kim, Vijaya Puri

PII: S1385-8947(18)31588-2
DOI: https://doi.org/10.1016/j.cej.2018.08.114
Reference: CEJ 19728

To appear in: *Chemical Engineering Journal*

Received Date: 21 April 2018
Revised Date: 14 August 2018
Accepted Date: 17 August 2018

Please cite this article as: G. Kulkarni, P. Kandesar, N. Velhal, V. Phadtare, A. Jatratkar, S.K. Shinde, D-Y. Kim, V. Puri, Exceptional electromagnetic interference shielding and microwave absorption properties of room temperature synthesized polythiophene thin films with double negative characteristics (DNG) in the Ku-band region, *Chemical Engineering Journal* (2018), doi: https://doi.org/10.1016/j.cej.2018.08.114

Exceptional electromagnetic interference shielding and microwave absorption properties of room temperature synthesized polythiophene thin films with double negative characteristics (DNG) in the Ku-band region

Gopal Kulkarni[1], Priyanka Kandesar[1], Ninad Velhal[1], Varsha Phadtare[1], Aviraj Jatratkar[1]**

S. K. Shinde[2], Dae-Young Kim[2], Vijaya Puri[1]*

[1]Thick and Thin Film Device laboratory, Department of Physics,

Shivaji University, Kolhapur - 416004, India

[2]Department of Biological and Environmental Science, College of Life Science and Biotechnology, Dongguk University-Ilsan, Biomedical Campus, Goyang-si, Gyeonggi-do, 410-773, Korea

Email: vrp_phy@unishivaji.ac.in*

Email: ninadvelhal@gmail.com**

ABSTRACT

Negative refractive index (NRI) metamaterials with simultaneously negative permittivity and negative permeability have recently experienced tremendous fundamental and practical interest due to their unique electromagnetic properties. In this work, polythiophene (PTh) thin films were synthesized using an in situ chemical oxidative polymerization route. The double negative characteristics (negative permittivity and permeability) appeared simultaneously in the as-prepared PTh thin films. The structural and microstructural characterizations of as-deposited PTh thin films were examined through different techniques including XRD, FESEM, TEM, XPS and FT-IR spectroscopy. Furthermore, microwave absorption properties such as reflection loss (RL), shielding effectiveness (SE) of the PTh thin films with

varying monomer concentration were also investigated. The morphological investigation shows that the unique porous microstructure of the PTh fibers has a dramatic impact in the enhancement kinetics of the microwave absorption performance. The PTh fibers deposited at 0.2 M concentration of thiophene showed minimum reflection loss (RL) of -44.24 dB (99.9% microwave absorption) at 17.59 GHz frequency, with a total shielding effectiveness of -18 dB at 16.3 GHz with only 5.31 microns of matching thickness. The PTh thin films exhibit exceptional microwave absorption ability at a fairly thin thickness and show a greater effective absorption bandwidth (RL < -10 dB) in the Ku-band region; these findings definitely pave the way to explore the study of different conducting polymer materials for utilization in EMI-shielding applications.

Keywords: Conducting polymers; Polythiophene (PTh); Metamaterial; Microwave absorption; EMI shielding; Relative Permittivity and permeability

Corresponding Author:
Dr. Vijaya Puri
Thick and Thin Film Device Lab. Department of Physics,
Shivaji University, Kolhapur, India -416004
Email: vrp_phy@unishivaji.ac.in
Fax No: 0091-231-2691533.
Phone No: 0091-231-2609230

Co- Corresponding author
Dr. Ninad Velhal
Thick and Thin Film Device Lab. Department of Physics,
Shivaji University, Kolhapur, India -416004
Email: ninadvelhal@gmail.com

1. Introduction

Recently, double negative index materials have attracted a great deal of attention across the globe due to their fascinating properties such as negative refraction, perfect absorption, and perfect transmission[1]. Due to these particular characteristics, metamaterials can be applied to various fields such as super lenses, optical cloaking and microwave antennae[2,3]. Moreover, a perfect metamaterial absorber, which can absorb electromagnetic waves, can be applied as a plasmonic sensor, solar cell, photodetector, thermal emitter and thermal imager[4,5]. The materials that show DNG characteristics can suppress electromagnetic waves generated by advanced electronic gadgets that are used daily such as cellular phones, laptops, local area networks, Wi-Fi and home appliances. The rapid use of these electronic gadgets is very harmful for mankind[6]. Furthermore, DNG materials provide a stealth function for avoiding radar detection to a military unmanned aerial vehicle, fighter, tank and warship[6]. These strengths have highly motivated researchers to explore applications of DNG materials in the various fields of materials science research.

The rapid growth in wireless information technology, especially in the high-frequency range, has led to a new kind of pollution: electromagnetic interference (EMI)[7,8]. This massive improvement in electronic gadgets and telecommunications has prompted significant concerns with regards to electromagnetic interference pollution (EMI)[9]. A key answer to tackle this problem is to fabricate types of materials that can suppress the undesirable electromagnetic waves[10,11] Electromagnetic interference not only can cause operational malfunction but can also produce adverse effects on human

health[12,13]. Persuaded by environmental questions and human health, the quest for materials with high efficiency to mitigate electromagnetic noise is a mainstream field of research[14,15].

Metals are effective materials widely applied in the shielding industry, but heavy weight, corrosion susceptibility and incommodious processing methods make these materials inappropriate for use in a shielding mechanism[16]. As lightweight materials and flexibility are crucial considerations, especially for military and aviation applications, tremendous efforts are presently ongoing for developing a suitable EMI shielding material on an industrial scale[17,18]. Ideal microwave absorption materials require low density and low thickness that show a strong microwave absorption over a wide frequency range[19][20].

Conducting polymers (CPs) represent a novel class of materials possessing a unique combination of electrical and mechanical properties that are useful for the suppression of electromagnetic noise[21]. Also the microwave properties of CPs cover wide area of application such as a coating in reflector antennae, RADAR, coating on flying objects (airplane) as a stealth material, frequency selective surfaces, satellite communication links, and microwave absorbing materials[22,23]. On the other hand, the properties of CPs such as their light weight, corrosion resistance, low toxicity, high conductivity, ease and high flexibility in preparation also render them as a potential candidate to replace conventional metals such as Fe, Co, Ni[24].

However, it was also found that the shielding effectiveness of CPs partially arises from their available microwave absorption performance rather than just from

reflection. This valid absorption performance motivated a great deal of research work on developing novel microwave absorbing materials (MAMs) based on various CPs[25]. Although the microwave absorption ability and shielding effectiveness properties of CPs have been studied earlier by some researchers, the performance of pure CPs is not so much exciting due to impedance mismatch and narrow absorption bandwidth. Chandrasekhar et al. investigated the microwave absorption and shielding properties of bulk polyaniline (PANI) in the frequency range 4-18 GHz and found shielding effectiveness approximately -15 dB, but poor absorption performance only up to -5 dB in the X and K bands[25]. Xie et al. designed an ultralight, three-dimensional (3D) polypyrrole (PPy) aerogel and (3D) polypyrrole/poly3,4-ethylenedioxythioxythiophene) (PPy/PEDOT) hybrid composite by a facile self-assembled polymerization method, with an effective EM absorption bandwidth (<−10 dB, 90% absorption) that could reach up to 6.2 GHz. Velhal N, Patil N, et al. reported the synthesis of a Ppy/PANI composite using galvanostatic electro polymerization and studied its electromagnetic properties study in the 8-18 GHz region. Many reports are available for the microwave absorption properties of Ppy and PANI, but PTh as a microwave absorber has not been intensively studied. Seyed Hossein Hosseini and Maryam Moloudi synthesized polythiophene nanofibers and reported a minimum reflection loss of -6 dB at 6 GHz and -8.5 dB at 14 GHz[26]. However, no reports are available on the microwave absorption properties of pure PTh thin films.

In the present manuscript, we report the facile synthesis of porous PTh thin films on an alumina substrate using a very simple and cost effective chemical bath

deposition method, and study their microwave absorption properties in the Ku band (12-18 GHz) region. Herein, effort has been made to develop unique microstructures of PTh such as hollow/porous. It is well accepted that the unique porous structure is favorable in the enhancement kinetics of microwave absorption phenomena. The porous structures, which let more microwaves penetrate into absorbing materials, can be used to tailor the complex permittivity and improve the impedance match between air and absorber,[27,28] also the porous structures can lead to multiple reflection and scattering phenomenon for incident microwaves inside the absorbing material, which results in attenuation of electromagnetic (EM) energy[25,29]. To the Author's knowledge, we have observed for the first time DNG behavior for PTh thin films.

2. Experimental section

2.1 Materials

AR grade chemicals were used for synthesis. Thiophene (AR grade Merck), $FeCl_3$ (98% Sd-Fine) were supplied by Fume Chemicals Co., Ltd. chloroform (CH_3Cl), and methanol (CH_3OH) were purchased from Sigma-Aldrich. All chemicals were used without any further purification, whereas alumina substrates were used for the preparation of PTh thin films.

2.2 Preparation of polythiophene thin films

The monomer solution was prepared by dissolving 0.1 M concentration of thiophene in chloroform, while oxidant solution was prepared using 0.4 M concentration of $FeCl_3$ in chloroform in a separate beaker. The monomer

concentration was varied from 0.1 to 0.5 M in steps of 0.1 to study the effect of the concentration on the microwave absorption properties of PTh thin films, whereas the oxidant concentration was kept constant at 0.4 M throughout all the experiments.

The substrates were immersed in a solution bath at room temperature with constant stirring. The monomer solution was added dropwise to the oxidant solution under the N_2 atmosphere. After some time, a brown colored precipitate was observed in the solution bath. During the precipitation, a heterogeneous reaction occurred and the deposition of PTh took place on the alumina substrate. The substrates coated with PTh thin films were removed from the bath after a time interval of 1 hour, washed repeatedly with methanol followed by chloroform and acetone to remove residual oxidant and unreacted monomers, dried in air and finally preserved in an airtight container.

3. Characterization

The XRD pattern for the PTh powder was obtained with a Bruker D2Phaser X-ray diffractometer using Cu − Kα radiation (λ=1.5418 Å). Scanning was carried out in the 2θ range from 0° to 90° at a scan rate of 10° per minute. The surface morphology of the as-prepared polythiophene thin films was investigated by field-emission scanning electron microscopy (FE-SEM, JEOL JSM 6390). FT-IR spectra for the polythiophene powder were recorded using a Perkin–Elmer spectrometer in the range of 500–4000 cm^{-1}. The room temperature DC electrical conductivity of the samples was measured by a two-probe method. Transmission electron

microscopy (TEM) analysis was carried out using a field emission transmission electron microscope, (TEM; Titan G2 ChemiSTEM Cs Probe) and XPS analysis was carried out using (XPS; ULVAC-PHI Quantera SXM.)

4. The growth mechanism for the PTh thin films

The chemical oxidative polymerization route has been selected to deposit PTh thin films. Chloroform ($CHCl_3$) is used as a solvent, whereas iron tri-chloride ($FeCl_3$) is used as an oxidant. In the chemical oxidative polymerization process mainly two steps are of prime importance for the film formation, i.e., nucleation and particle growth. Nucleation is a heterogeneous process in which decomposition of the monomer molecules takes place in the solution and forms an active layer on the substrate surface[30]. When the clusters of the molecules formed undergo rapid decomposition, a heterogeneous reaction occurs and particles start to combine and grow on the substrate surface up to a certain film thickness[31]. The film thickness is dependent on the molar concentration of monomer and oxidant, deposition time, temperature of the bath, the stirring rate, etc.

Herein, all the experiments were carried out at room temperature. All other parameters were held constant, with only the molar concentration of the monomer varied from 0.1 to 0.5 M to study the effect of it on the thickness and microwave absorption performance of PTh thin films. It is important to note that at 0.1 M concentration, no film formation is found on the alumina substrate surface due to the low concentration of monomer. However, at higher concentrations of monomer, well-adhered PTh films were formed on the alumina substrates. The thickness of the

films decreases with increasing monomer concentration. A maximum thickness of 5.31 microns was achieved at a thiophene concentration of 0.2 M. The PTh thin film deposition takes place as described in the following steps.

After addition of the monomer solution to the oxidant solution, the free radicals of the Fe^{3+} ions interface with one of the π electrons in the monomer molecules and forms a normal pair of electrons, transferring another π electron to another monomer molecule, which results in linking of the second monomer to the first and the polymerization[32]. The possible reaction and growth mechanism for PTh thin film formation is shown in Figure 1.

5. Results and discussion

5.1 XRD analysis

Figure 2a depicts the XRD pattern for the PTh powder scratched from the alumina substrate. The data exhibit only one broad peak showing the amorphous nature of the formed PTh fibers. The diffraction peaks centered at 26.5° and 39.7° are strongly associated with the intermolecular π-π stacking structure in polythiophene chains[33].

5.2 FT-IR Spectroscopy

To determine the nature of the chemical bonding and successful formation of polythiophene, an FT-IR study was carried out in the range 500 to 4000 cm^{-1}. Figure 2b shows the FT-IR spectra for PTh powder scratched from the alumina substrate. The absorption peak centered at 692 cm^{-1} is attributed to the C-S

stretching in the thiophene ring, while the peak centered at 790 cm^{-1} is due to the C-H out of plane vibration of the 2-5-substituted thiophene ring created by polymerization of the thiophene monomer[34]. The peak observed at 1030 cm^{-1} is assigned to the in-plane stretching vibration of C-H[35]. The absorption bands at 1501 cm^{-1} and 1634 cm^{-1} arise due to C-C stretching vibrations and C=C symmetric stretching vibrations of the thiophene ring, respectively[36]. The peak present at 1844 cm^{-1} was assigned to the C=O bond that concludes the inclusion of the small amount of oxygen in a film. The bands centered between 2872–3063 cm^{-1} are attributed to the C-H stretching vibration[34]. The present FT-IR result clearly indicates polymerization of the thiophene monomer.

5.3 FESEM analysis

Figure 3a shows FESEM images of the PTh thin films deposited at various concentrations of thiophene. It is seen that the PTh thin films show different morphologies as the monomer concentration changes. The PTh film deposited at a thiophene concentration of 0.2 M shows a very porous surface morphology with nanosized particles uniformly distributed over a large surface area. Additionally, at 0.3 M concentration of thiophene, a highly agglomerated, porous and well-interconnected grain structure for the PTh nanoparticles is observed. However, at 0.4 M and 0.5 M concentration of thiophene, the morphology of the PTh samples changes dramatically, with uneven growth of the PTh nanoparticles.

5.4 TEM analysis

Figure 3b shows the TEM images of the PTh thin films deposited at various monomer concentrations. It is clearly seen that a fibrous and porous morphology is observed in the as-prepared PTh thin films, which is also in good agreement with the FESEM analysis. The black portion seen in the TEM images suggests the presence of a porous network of polythiophene nanoparticles. The PTh thin films deposited at 0.2 M and 0.3 M concentration of thiophene show a very compact morphology compared to the films deposited at 0.4 M and 0.5 M concentration. The average particle size of the PTh nanoparticles was found to be in the range of ~ 40-60 nm.

5.5 XPS analysis

Figure 4a shows the survey scan XPS spectra for the polythiophene thin film, while Figure 4b shows the narrow scan XPS spectra of the C1s core level. The XPS spectra for the S2p core level is shown in Figure 4c. The survey scan spectra depict the presence of distinct bands at binding energies corresponding to the Si2p, S2p, Cl2p, C1s, N1s, and O1s core levels[37]. The peak present at 284.5 eV is attributed to C1s, which is in good agreement with the standard carbon signal showing almost the same binding energy 284.6 eV[31]. The deconvoluted graph for C1s shows two distinct peaks, which are attributed to the C-C, C=C, C-H bonds at B.E. 284.5eV and C-S bond at B.E. 286.5 eV. The peak present at 284.5eV is associated with α and β carbon atoms in the polymeric chains[38], whereas the presence of the C-S band at 286.5 eV confirms the successful deposition of polythiophene[31]. The core-level N1s spectra show the presence of free amine along with a secondary amine peak at 399.2 eV and a protonated amine peak at 400.8 eV[37]. The

deconvoluted S2p core level spectra also show two distinct peaks corresponding to $S2p_{3/2}$ and $S2p_{1/2}$ core levels at different binding energies. The $S2p_{3/2}$ and $S2p_{1/2}$ peaks were observed at 167.79 eV and 168.89 eV respectively.

Actually, according to the NIST database for XPS, the peak position for the S2p orbit in the thiophene should be approximately at 164 eV[39]. However, herein, a huge shift in the binding energies for the S2p orbit is observed. The origin for the binding energy shift is “surface effects”. For pure “S”, the bandwidth at the surface of S is presumed to be narrower for the surface layer due to the reduction in neighboring atoms. Therefore, the narrowing of the p-band at the surface requires charge transfer to align the Fermi levels. Hence, the surface atom acquires a net positive charge relative to the bulk atom and the surface core level shifts to higher binding energies. However, the energy difference in the $S2p_{3/2}$ and $S2p_{1/2}$ peaks is 1.1 eV, which is close to the expected value of 1.17 eV[31].

6. Room temperature DC conductivity and thickness study

Room temperature DC conductivity values for the PTh samples deposited at various monomer concentrations of thiophene measured by a two-point probe method are tabulated in table 1 along with results from a thickness study of the samples carried out using a digital microbalance. It is seen that the PTh thin film thickness decreases with increasing monomer concentration. Generally, the most accepted mechanism is that as the monomer concentration increases, the film thickness also increases. In the case of the 0.1 M concentration, no reaction between monomer and oxidant occurs, resulting in no PTh film formation. While at

0.2 M concentration of thiophene, a precipitate was slowly formed in the reaction bath. Thus, a nucleation process and particle growth of PTh nanoparticles on the alumina substrate was obtained in a well-ordered manner, resulting in dark-brownish PTh thin film formation. The ratio of monomer to oxidant is exactly matched to obtain a well adhered PTh thin film at 0.2 M concentration. However, as the thiophene concentration increases to 0.3 M, the reaction rate increases drastically, with sudden precipitation occurring in the reaction bath. Here, also, a thick layer of PTh is primarily observed on the alumina substrate; however, the upper layer peels off when it is washed with chloroform due to loose bonding of molecules with the substrate. Additionally, at 0.4 and 0.5 M concentration, similar behavior is observed. Hence, the sample deposited at 0.2 M concentration of thiophene shows the highest thickness of 5.31 microns and the highest electrical conductivity of 5.412×10^{-3} S/m. As the thickness decreases, the DC conductivity of the samples also decreases at higher monomer concentrations. Figure 5 shows a picture of the PTh samples deposited at various concentrations of thiophene.

7. Measurement of the microwave parameters

The samples were cut into the desired rectangular shape, i.e., height a=1.8 cm and width b=1 cm, to fit into a Ku-band waveguide adapter, with the whole assembly connected to an Agilent Vector Network Analyzer using co-axial cables for microwave property measurements. Full two-port calibration was performed to remove errors. The S-parameters (S_{11} and S_{21}) are the basic building blocks to determine the microwave parameters of the material under test (MUT). Two coaxial rectangular waveguide adapters, (Ku-band 12-18 GHz) filling completely the fixture

cross section, were used to determine the S-parameters of the MUT. The complex scattering parameters S_{11} and S_{21}, corresponding to reflection and transmission, were measured using the VNA and used to study the reflection loss, shielding effectiveness of the polythiophene thin films. After the S-parameter measurements, the real and imaginary parts of the permittivity and permeability of the MUT (ε', ε'' and μ', μ'') were calculated according to the standard Nicholson Ross Weir (NRW) algorithm[40].

7.1 Reflection loss

Figure 6 illustrates the variation of the reflection loss (dB) with frequency in the 12-18 GHz (Ku-Band) frequency region for varying concentrations of thiophene monomer. Reflection loss (RL) of the PTh thin films was calculated from the complex scattering parameter (S_{11}), obtained directly from the Agilent Vector Network Analyzer PNA 5230, which is expressed as,[41]

$$RL = 20 * \log |S_{11}| \quad \text{..... (1)}$$

The RL plots for the PTh thin films cover the broad frequency bandwidth of the Ku-band region. All the PTh thin films deposited at various monomer concentrations show effective attenuation (RL< -20 dB) in the Ku-band region. The minimum RL value observed in the PTh film deposited at 0.2 M concentration of thiophene was up to -44.41 dB, i.e., (99.99% microwave absorption) at 17.54 GHz, which is higher than the value reported in earlier studies, with a matching thickness of only 5.31 microns. A possible reason for the higher microwave absorption should be the porous structure of the PTh fibers, which can assist multiple

reflection/scattering phenomena[25,42] inside the pores of the PTh fibers, resulting in an enhanced RL value at 17.54 GHz. The observed values of RL for 0.3 M concentration at different frequencies are also exciting: -39.14, -15.11 and -16.47 dB. The RL values drop to a lower order at 0.4 and 0.5 M concentration of thiophene: -26.5 dB and 26 dB at 12.3 and 14.9 GHz frequency, respectively. The thickness of the absorbent also plays a crucial role in the enhancement kinetics of the microwave absorption performance[18]. At higher concentrations, i.e., at 0.4 M and 0.5 M concentration, the thickness of the films decreases due to the occurrence of sudden precipitation in the reaction bath. This could be a possible reason for the lower microwave absorption performance at higher concentrations of monomer.

8. Mechanism for EMI shielding

The EMI shielding phenomenon is basically dependent on three primary mechanisms: reflection from the shield, absorption of electromagnetic energy and multiple internal reflection of electromagnetic radiation[43]. Figure 8 shows a graphical representation of the shielding mechanism. An effective EMI shielding material must both reduce undesirable emission and safeguard the component from stray signals. The primary function of EM shields is to reflect radiation, utilizing charge carriers that interact especially with the EM fields[44]. Therefore, shielding materials ought to be electrically conductive. Regardless, conductivity is not the only prerequisite. A secondary mechanism of EMI shielding is the absorption of electromagnetic radiation, which is caused by the interaction of electromagnetic radiation with electric/magnetic dipoles, electrons and phonons present in the material[45]. The high electrical conductivity of the shield is an essential variable

for clearly determining the microwave absorption phenomena. Additionally, the other properties of shield materials such as thickness, electrical permittivity and magnetic permeability are crucial parameters that determine the ultimate shielding performance. However, a third phenomenon, multiple internal reflections in the materials, also contributes noticeably to EMI shielding effectiveness. These internal reflections originate from the scattering centers and interfaces or defect sites within the shielding material, resulting in multiple scattering and absorption of EM waves[44]. Hence, the total shielding effectiveness is the sum of the contributions from absorption, reflection, and transmission or multiple internal reflections. The SE_R, i.e., shielding due to reflection, is related to the impedance mismatch between the air and shielding material, whereas SE_A, i.e., shielding due to absorption, is the energy dissipation of the electromagnetic microwaves in the shield[46], and SE_M, i.e., absorption of the EM energy, associated with multiple internal reflections. Therefore, the total shielding effectiveness of any shield can be expressed as,[47]

$$SE_T = SE_A + SE_R + SE_M \quad \text{..... (2)}$$

S parameters of the two-port network analyzer, i.e., S_{11} (S_{22}) and S_{21} (S_{12}) represent the reflection and transmission coefficients given as follows[48]:

$$R = |S_{11}|^2 = |S_{22}|^2 \quad \text{..... (3)}$$

$$T = |S_{21}|^2 = |S_{12}|^2 \quad \text{..... (4)}$$

The absorption coefficient can be simply expressed as,

$$A + R + T = 1 \quad \text{..... (5)}$$

Total shielding effectiveness can be conveniently expressed in terms of S parameters as,

$$SE_T = 20 * \log |S_{21}| \quad \text{..... (6)}$$

The SE_M term in equation (1) can be ignored for practical applications when SE_T > -10 dB; thus, equation (1) can be reduced to[49],

$$SE_T = SE_A + SE_R \quad \text{..... (7)}$$

Furthermore, SE_A and SE_R are obtained directly from the following equations,

$$SE_A = 10 \log \left(\frac{10^{\frac{S21}{10}}}{1-10^{\frac{S11}{10}}} \right) \quad \text{..... (8)}$$

$$SE_R = 10 \log (1 - 10^{\frac{S11}{10}}) \quad \text{..... (9)}$$

9. Shielding effectiveness study

The variation of SE_T, SE_A and SE_R in the 12-18 GHz frequency range is shown in Figure 7a. Thus, a minimum SE_T is observed for the PTh thin film, which is deposited at 0.2 M concentration of thiophene. The observed value for SE_T is ~18 dB, which is far below the -10 dB bandwidth and could meet the requirement for use in practical applications. At higher concentrations, a slight decrement is observed in the shielding effectiveness performance of PTh thin films, but overall a good shielding response is observed for all the PTh thin films deposited at various concentrations of monomer in the Ku-band region. Figure 7b shows the shielding effectiveness due to absorption, i.e., SE_A varies from ~ -7 dB to -4.0 dB, but shielding effectiveness due to reflection, Figure 7c, i.e., SE_R, contributed very little,

showing a nominal value that lies between -1 to -5 dB, which suggests that the shielding effectiveness due to multiple internal reflections, i.e., $SE_{M,}$ is greater. The porous morphology of PTh thin films observed from FESEM and TEM analysis could be the reason for the facilitation of the multiple internal reflection phenomenon inside the material, resulting in an enhanced microwave absorption performance in the 12-18 GHz region.

10. Polythiophene with negative permittivity and permeability

Normally, the microwave absorption behavior of materials is dependent on the relative permittivity and permeability. However, due to the nonmagnetic nature of PTh, the microwave absorption behavior is only related to the relative permittivity. The small negative permittivity and tuned electrical conductivity indicate that a more disordered motion of the charge carriers along the backbone of the PTh polymer prompted enhanced microwave behavior in PTh thin films.

Generally, permittivity is the measure of resistance that is encountered when forming an electric field in a medium. Permittivity is a complex quantity, which describes the interaction of a material with an electric field E[50]. The dielectric constant (k) is equivalent to the relative permittivity (ε_r') or absolute permittivity (ε) relative to the permittivity of free space (ε_o). The real part of the permittivity (ε_r') indicates how much energy from an external electric field is stored in a material, while the imaginary part of the permittivity (ε_r'') is called the loss factor and is a measure of how dissipative or lossy a material is to an external electric field[51]. Permittivity is directly related to electric susceptibility, which is a measure of how easily a dielectric polarizes in response to an electric field. Thus,

permittivity relates to a material's ability to resist an electric field. Figure 9 shows the relative permittivity plots with respect to frequency for PTh thin films deposited at various concentrations of thiophene. The imaginary part of the permittivity (ε_r'') for 0.2 M concentration of thiophene varies from 1.3 to 0.8, but most of the frequency region shows a small negative permittivity, which varies in between -0.4 to -0.2. Additionally, in the case of 0.3 M concentration of thiophene, (ε_r'') varies from +2 to -2.5. The real part of the permittivity (ε_r') shows a transition from a positive to negative value. The metallicity of the materials and the plasma oscillation of delocalized electrons may lead to negative permittivity in polythiophene. In the case of metals, the carrier concentration is extremely high, which leads to a large negative permittivity; however, it is believed that conductive materials with relatively moderate carrier concentration are the most prominent alternatives for metals and are more beneficial to achieve weakly negative permittivity behavior in a wide frequency region[52]. Conducting polymers such as PANI, PTh possess moderate carrier concentration compared to metals. Herein, also, the continuous conducting pathway formed by porous PTh represents an intrinsic metallic state of the formed material[53]. Thus, the concentration of delocalized electrons (N) is obviously larger in the PTh chain. Hence, the motion of charge carriers is more disordered along the backbone of the PTh chain due to the plasma oscillations of the delocalized electrons[54]. If the concentration of delocalized electrons (N) is more, then, the plasma frequency is definitely greater than the frequency of the electric field, i.e., $\omega_p > \omega$. Below the plasma frequency, the dielectric function is negative and the field cannot penetrate the sample. Hence,

if the frequency of the electric field (ω) is less than the plasma frequency (ω_p) then there is generation of negative permittivity.[55] The meaning of negative permittivity is related to the nonresistance of the material to electric field. Slight variations are observed in the (ε_r') and (ε_r'') values at 0.4 M and 0.5 M concentrations of thiophene.

Permeability is also a complex quantity (μ), which describes the interaction of a material with a magnetic field. The permeability (μ) consists of a real part (μ') that represents the energy storage term and an imaginary part (μ'') representing the energy loss term[50].

Figure 10 depicts the relative permeability plots of PTh thin films with respect to frequency deposited at various concentrations of thiophene. As polythiophene is a nonmagnetic material, it does not show any huge variation in the permeability values for all the samples. The real part of the permeability shows very little variation for 0.2 M concentration of thiophene, it varies only from 0.08 to 0.15. However, the imaginary part shows a small negative permeability, which varies from -0.14 to +0.15. The negative permeability in PTh thin films is attributed to plentiful conductive loops due to the porous structure of PTh fibers. These PTh nanoparticles are compactly packed and directly connected, which leads to a large number of micro pores and conductive loops around the micro pores, as revealed from Figure 3a. At 0.2 M and 0.3 M concentrations, PTh nanoparticles are well interconnected to each other, which is the reason in particular for obtaining higher electrical conductivity values at these two concentrations. A porous structure leads to an increase in the number of conductive loops. In a high-frequency

electromagnetic field, a large number of ring currents are generated in the conductive loops to resist the external magnetic field. When the superimposed magnetic field generated by each ring current is greater than the external magnetic field, a negative magnetic permeability is generated[56].

11. Microwave Attenuation

It is well known that to enhance the higher attenuation ability in materials, magnetic and dielectric losses should be as high as possible. In the absence of magnetic losses, dielectric loss is the most prominent factor for better attenuation capability. Figure 11 shows plots of microwave attenuation for the PTh thin films deposited at various monomer concentrations in the 12–18 GHz frequency region. Microwave attenuation was calculated from the following formula[35],

$$Attenuation\ (dB) = 10\ log_{10}\ \frac{Input\ power\ (watt)}{Output\ power\ (watt)}$$

It is seen from Figure 11 that the microwave attenuation for the PTh thin films decreases gradually as the concentration of monomer increases. A maximum microwave attenuation was observed for the PTh thin film deposited at 0.2 M concentration of thiophene, with a value of approximately 22 dB at 16.2 GHz. Later, at higher concentrations of monomer, a substantial decrement was observed in the attenuation values. The possible reason for this observation would be the lower thickness of the absorbent, with an agglomerated structure observed in the FESEM analysis of PTh thin films at higher monomer concentrations.

12. Conclusions

In summary, we investigated the microwave absorption and shielding effectiveness properties of PTh thin films showing a small negative permittivity and negative permeability, i.e., DNG behavior for as-prepared thin films observed in the Ku-band region. The XRD pattern demonstrated the amorphous nature of PTh. The morphological investigation shows that a porous fibrous structure is a possible reason for the excellent microwave absorption performance observed in the Ku-band region. The presence of distinct bands at their particular binding energies in the XPS spectra confirms the successful deposition of polythiophene. The PTh thin film shows a minimal RL value of -44.41 dB and a shielding effectiveness of -18.02 dB with only a few micrometers of matching thickness. The microwave absorption properties of some CPs and polymer-based nanocomposites reported recently are listed in Table 2. It can be seen that our PTh thin films show a relatively lower RL, broader bandwidth, considerable attenuation and thinner matching thickness compared to those of the reports published earlier. Additionally, the DNG characteristics of the PTh thin films will motivate scientists to investigate the double negative property in other polymer nanocomposites. These findings open up a practicable pathway to tune the microwave absorption in a wide frequency bandwidth. On the other hand, the properties of PTh thin films such as low matching thickness, light weight, easy preparation and wideband microwave absorption could meet the requirement for use at the commercial level for shielding purposes.

Acknowledgement

One of the authors, Vijaya Puri, gratefully acknowledges UGC New Delhi, for the award of Research Scientist “C”. The author Gopal Kulkarni acknowledges DST-SERB for providing JRF under the project No. [SERB/F/2139/2016-17]. All the authors also thank UGC-SAP, DST-FIST and PIFC (Physics Instrumentation Facility Centre), Department of Physics, SUK for their assistance.

References:

[1] N.I. Landy, S. Sajuyigbe, J.J. Mock, D.R. Smith, W.J. Padilla, Perfect metamaterial absorber, Phys. Rev. Lett. 100 (2008) 1–4. doi:10.1103/PhysRevLett.100.207402.

[2] L.W. Li, Y.N. Li, T.S. Yeo, J.R. Mosig, O.J.F. Martin, A broadband and high-gain metamaterial microstrip antenna, Appl. Phys. Lett. 96 (2010). doi:10.1063/1.3396984.

[3] D. Schurig, J.J. Mock, B.J. Justice, S.A. Cummer, J.B. Pendry, A.F. Starr, D.R. Smith, Metamaterial electromagnetic cloak at microwave frequencies, Science (80). 314 (2006) 977–980. doi:10.1126/science.1133628.

[4] N. Liu, M. Mesch, T. Weiss, M. Hentschel, H. Giessen, Infrared perfect absorber and its application as plasmonic sensor, Nano Lett. 10 (2010) 2342–2348. doi:10.1021/nl9041033.

[5] X. Liu, T. Tyler, T. Starr, A.F. Starr, N.M. Jokerst, W.J. Padilla, Taming the blackbody with infrared metamaterials as selective thermal emitters, Phys. Rev. Lett. 107 (2011) 4–7. doi:10.1103/PhysRevLett.107.045901.

[6] Y.J. Yoo, S. Ju, S.Y. Park, Y. Ju Kim, J. Bong, T. Lim, K.W. Kim, J.Y. Rhee, Y.P. Lee, Metamaterial absorber for electromagnetic waves in periodic water droplets, Sci. Rep. 5 (2015) 3–10. doi:10.1038/srep14018.

[7] F. Wen, F. Zhang, Z. Liu, Investigation on Microwave Absorption Properties for Multiwalled Carbon Nanotubes / Fe / Co / Ni Nanopowders as Lightweight Absorbers, J. Phys. Chem. C. 115 (2011) 14025–14030. doi:10.1021/jp202078p.

[8] Y. Lin, J. Dai, H. Yang, L. Wang, F. Wang, Graphene multilayered sheets assembled by porous $Bi_2Fe_4O_9$ microspheres and the excellent electromagnetic wave absorption properties, Chem. Eng. J. 334 (2018) 1740–1748. doi:10.1016/j.cej.2017.11.150.

[9] H. Wang, C.-E. Huang, Z. Cui, C. Shen, Microwave dielectric properties of $0.6ZrO_2$–$0.4(Zn_{1/3}Nb_{2/3})$ O_2–TiO_2 ceramics doped with Li_2CO_3, CuO or $MnCO_3$, J. Mater. Sci. Mater. Electron. 29 (2018) 2–9. doi:10.1007/s10854-017-7880-8.

[10] S. Biswas, Y. Bhattacharjee, S.S. Panja, S. Bose, Graphene oxide co-doped with dielectric and magnetic phases as an electromagnetic wave suppressor, Mater. Chem. Front. 1 (2017) 1229–1244. doi:10.1039/C6QM00335D.

[11] L. Wang, X. Bai, M. Wang, Facile preparation, characterization and highly effective microwave absorption performance of porous α-Fe_2O_3 nanorod–graphene composites, J. Mater. Sci. Mater. Electron. 0 (2017) 1–10. doi:10.1007/s10854-017-8273-8.

[12] N. Joseph, J. Varghese, M.T. Sebastian, A facile formulation and excellent electromagnetic absorption of room temperature curable polyaniline nanofiber based inks, J. Mater. Chem. C. 4 (2016) 999–1008. doi:10.1039/C5TC03080C.

[13] X.X. Wang, T. Ma, J.C. Shu, M.S. Cao, Confinedly tailoring Fe_3O_4 clusters-NG to tune electromagnetic parameters and microwave absorption with broadened bandwidth, Chem. Eng. J. 332 (2018) 321–330. doi:10.1016/j.cej.2017.09.101.

[14] N. Abbas, H.T. Kim, Multi-walled carbon nanotube/polyethersulfone nanocomposites for enhanced electrical conductivity, dielectric properties and efficient electromagnetic interference shielding at low thickness, Macromol. Res. 24 (2016) 1084–1090. doi:10.1007/s13233-016-4152-z.

[15] L. Wang, J. Zhu, H. Yang, F. Wang, Y. Qin, T. Zhao, P. Zhang, Fabrication of hierarchical graphene@Fe_3O_4@SiO_2@polyaniline quaternary composite and its improved electrochemical performance, J. Alloys Compd. 634 (2015) 232–238. doi:10.1016/j.jallcom.2015.02.062.

[16] M. Verma, S.S. Chauhan, S.K. Dhawan, V. Choudhary, Graphene nanoplatelets/carbon nanotubes/polyurethane composites as efficient shield against electromagnetic polluting radiations, Compos. Part B Eng. 120 (2017) 118–127. doi:10.1016/j.compositesb.2017.03.068.

[17] A. Kumar, A.P. Singh, S. Kumari, A.K. Srivastava, S. Bathula, S.K. Dhawan, P.K. Dutta, A. Dhar, EM shielding effectiveness of Pd-CNT-Cu nanocomposite buckypaper, J. Mater. Chem. A. 3 (2015) 13986–13993. doi:10.1039/C4TA05749J.

[18] C.Y. Chen, N.W. Pu, Y.M. Liu, S.Y. Huang, C.H. Wu, M. Der Ger, Y.J. Gong, Y.C. Chou, Remarkable microwave absorption performance of graphene at a very low loading ratio, Compos. Part B Eng. 114 (2017) 395–403. doi:10.1016/j.compositesb.2017.02.016.

[19] N. Li, G.W. Huang, Y.Q. Li, H.M. Xiao, Q.P. Feng, N. Hu, S.Y. Fu, Enhanced microwave absorption performance of coated carbon nanotubes by optimizing the Fe_3O_4 nanocoating structure, ACS Appl. Mater. Interfaces. 9 (2017) 2973–2983. doi:10.1021/acsami.6b13142.

[20] J. Yan, Y. Huang, C. Wei, N. Zhang, P. Liu, Covalently bonded polyaniline/graphene composites as high-performance electromagnetic (EM) wave absorption materials, Compos. Part A Appl. Sci. Manuf. 99 (2017) 121–128. doi:10.1016/j.compositesa.2017.04.016.

[21] Y.J. Yim, K.Y. Rhee, S.J. Park, Electromagnetic interference shielding effectiveness of nickel-plated MWCNTs/high-density polyethylene composites, Compos. Part B Eng. 98 (2016) 120–125. doi:10.1016/j.compositesb.2016.04.061.

[22] K. Lakshmi, H. John, R. Joseph, K.E. George, K.T. Mathew, Comparison of microwave and electrical properties of selected conducting polymers, Microw. Opt. Technol. Lett. 50 (2008) 504–508. doi:10.1002/mop.

[23] X. Fan, J. Guan, W. Wang, G. Tong, Morphology evolution, magnetic and microwave absorption properties of nano/submicrometre iron particles obtained at different reduced temperatures, J. Phys. D. Appl. Phys. 42 (2009) 075006. doi:10.1088/0022-3727/42/7/075006.

[24] M. Verma, P. Verma, S.K. Dhawan, V. Choudhary, Tailored graphene based polyurethane composites for efficient electrostatic dissipation and electromagnetic interference shielding applications, RSC Adv. 5 (2015) 97349–97358. doi:10.1039/C5RA17276D.

[25] Y. Wang, Y. Du, P. Xu, R. Qiang, X. Han, Recent advances in conjugated polymer-based microwave absorbing materials, Polymers (Basel). 9 (2017). doi:10.3390/polym9010029.

[26] S.H. Hosseini, M. Moloudi, Preparation of nanofiber polythiophene layered on $Ba_xSr_{1-x}Fe_{12}O_{19}/Fe_3O_4$/polyacrylic acid core–shell structure and its microwave absorption investigation, Appl. Phys. A Mater. Sci. Process. 120 (2015) 1165–1171. doi:10.1007/s00339-015-9296-8.

[27] C. Ma, B. Zhao, Q. Dai, B. Fan, G. Shao, R. Zhang, Porous structure to improve microwave absorption properties of lamellar ZnO, Adv. Powder Technol. 28 (2017) 438–442. doi:10.1016/j.apt.2016.10.016.

[28] R. Bin Yang, P.M. Reddy, C.J. Chang, P.A. Chen, J.K. Chen, C.C. Chang, Synthesis and characterization of Fe_3O_4/polypyrrole/carbon nanotube composites with tunable microwave absorption properties: Role of carbon nanotube and polypyrrole content, Chem. Eng. J. 285 (2016) 497–507. doi:10.1016/j.cej.2015.10.031.

[29] Q. Ma, H.M. Zheng, Y. Shao, B. Zhu, W.J. Liu, S.J. Ding, D.W. Zhang, Atomic-Layer-Deposition of Indium Oxide Nano-films for Thin-Film Transistors, Nanoscale Res. Lett. 13 (2018) 4. doi:10.1186/s11671-017-2414-0.

[30] A.A. Jatratkar, J.B. Yadav, S. V. Kamat, V.S. Patil, D.B. Mahadik, H.C. Barshilia, V. Puri, R.K. Puri, Consequence of oxidant to monomer ratio on optical and structural

properties of Polypyrrole thin film deposited by oxidation polymerization technique, J. Phys. Chem. Solids. 80 (2015) 78–83. doi:10.1016/j.jpcs.2015.01.004.

[31] S. V. Kamat, J.B. Yadav, V. Puri, R.K. Puri, O.S. Joo, Characterization of poly (3-methyl thiophene) thin films prepared by modified chemical bath deposition, Appl. Surf. Sci. 258 (2011) 482–488. doi:10.1016/j.apsusc.2011.08.084.

[32] S. V. Kamat, V. Puri, R.K. Puri, Room temperature synthesis and characterization of polythiophene thin films by chemical bath deposition (CBD) method, Mater. Chem. Phys. 132 (2012) 228–232. doi:10.1016/j.matchemphys.2011.11.044.

[33] S. Sakthivel, A. Boopathi, Synthesis and Preparation of Polythiophene Thin Film by Spin Coating Method, J. Chemisitry Chem. Sci. 4 (2014) 150–155. doi:10.1016/j.snb.2005.10.019.

[34] D.B. Kamble, A.K. Sharma, J.B. Yadav, V.B. Patil, R.S. Devan, A.A. Jatratkar, M.A. Yewale, V. V. Ganbavle, S.D. Pawar, Facile chemical bath deposition method for interconnected nanofibrous polythiophene thin films and their use for highly efficient room temperature NO_2 sensor application, Sensors Actuators, B Chem. 244 (2017) 522–530. doi:10.1016/j.snb.2017.01.021.

[35] M. Nasrollahzadeh, M. Jahanshahi, M. Salehi, M. Behzad, H. Nasrollahzadeh, Synthesis and characterization of nanostructured polythiophene in aqueous medium by soft-template method, J. Appl. Chem. 08 (2013) 53–58. doi:10.1007/s40092-014-0068-4.

[36] M. Hatamzadeh, M. Jaymand, Synthesis and characterization of polystyrene-graft-polythiophene via a combination of atom transfer radical polymerization and Grignard

reaction, RSC Adv. 4 (2014) 16792–16802. doi:10.1039/C4RA01228C.

[37] S. Jayaraman, D. Rajarathnam, M.P. Srinivasan, Formation of polythiophene multilayers on solid surfaces by covalent molecular assembly, Mater. Sci. Eng. B Solid-State Mater. Adv. Technol. 168 (2010) 45–54. doi:10.1016/j.mseb.2010.01.052.

[38] S. V. Kamat, J.B. Yadav, V. Puri, R.K. Puri, Modification of the properties of polythiophene thin films by vapor chopping, Appl. Surf. Sci. 258 (2012) 7567–7573. doi:10.1016/j.apsusc.2012.04.088.

[39] https://srdata.nist.gov/xps/main_search_menu.aspx.

[40] A.M. Nicolson, Measurement of the Intrinsic Properties of Materials by Time-Domain Techniques _ R, (1970).

[41] G. Kulkarni, N. Velhal, V. Phadtare, V. Puri, Enhanced electromagnetic interference shielding effectiveness of chemical vapor deposited MWCNTs in X-band region, J. Mater. Sci. Mater. Electron. 28 (2017) 7212–7220. doi:10.1007/s10854-017-6402-z.

[42] H. Lv, X. Liang, G. Ji, H. Zhang, Y. Du, Porous three-dimensional flower-like Co/CoO and its excellent electromagnetic absorption properties, ACS Appl. Mater. Interfaces. 7 (2015) 9776–9783. doi:10.1021/acsami.5b01654.

[43] M.H. Al-saleh, EMI shielding effectiveness of carbon based nanostructured polymeric materials : A comparative study, Carbon 60 (2013) 146–156. doi:10.1016/j.carbon.2013.04.008.

[44] Y. Bhattacharjee, I. Arief, S. Bose, Recent trends in multi-layered architectures towards screening electromagnetic radiation: Challenges and perspectives, J. Mater. Chem. C. 5

(2017) 7390–7403. doi:10.1039/c7tc02172k.

[45] C.R.P. Patel, P. Tripathi, S. Singh, A.P. Singh, S.K. Dhawan, R.K. Kotnala, B.K. Gupta, O.N. Srivastava, New emerging radially aligned carbon nano tubes comprised carbon hollow cylinder as an excellent absorber for electromagnetic environmental pollution, J. Mater. Chem. C. 4 (2016) 5483–5490. doi:10.1039/C6TC00809G.

[46] S.R. Dhakate, K.M. Subhedar, B.P. Singh, Polymer nanocomposite foam filled with carbon nanomaterials as an efficient electromagnetic interference shielding material, RSC Adv. 5 (2015) 43036–43057. doi:10.1039/C5RA03409D.

[47] S. Pande, B.P. Singh, R.B. Mathur, T.L. Dhami, P. Saini, S.K. Dhawan, Improved electromagnetic interference shielding properties of MWCNT-PMMA composites using layered structures,Nanoscale Res. Lett. 4 (2009) 327–334. doi:10.1007/s11671-008-9246x.

[48] R. Panigrahi, S.K. Srivastava, Trapping of microwave radiation in hollow polypyrrole microsphere through enhanced internal reflection : A novel, Sci. Rep. 5 (2015) 7638. doi:10.1038/srep07638.

[49] K. Manna, S.K. Srivastava, V. Mittal, Role of Enhanced Hydrogen Bonding of Selectively Reduced Graphite Oxide in Fabrication of Poly (vinyl alcohol) Nanocomposites in Water as EMI Shielding Material, J. Phys. Chem. C. 120 (2016) 17011–17023. doi:10.1021/acs.jpcc.6b03356.

[50] Agilent Technologies, Solutions for Measuring Permittivity and Permeability with LCR Meters and Impedance Analyzers, Appl. Note. (2014) 1–5. doi:5980-2862EN.

[51] K.C. Yaw (Rohde&Schwarz), Measurement of dielectric material properties Application Note, Meas. Tech. (2006) 1–35.

[52] C. Cheng, R. Fan, L. Qian, X. Wang, L. Dong, Y. Yin, Tunable negative permittivity behavior of random carbon/alumina composites in the radio frequency band, RSC Adv. 6 (2016) 87153–87158. doi:10.1039/c6ra19591a.

[53] H. Gu, J. Guo, S. Wei, Z. Guo, Polyaniline nanocomposites with negative permittivity, J. Appl. Polym. Sci. 130 (2013) 2238–2244. doi:10.1002/app.39420.

[54] Y.N. Koh, N. Mokhtar, S.W. Phang, Effect of microwave absorption study on polyaniline nanocomposites with untreated and treated double wall carbon nanotubes, Polym. Compos. 16 (2016) 101–113. doi:10.1002/pc.24064.

[55] S. Anantha Ramakrishna, Physics of negative refractive index materials, Reports Prog. Phys. 68 (2005) 449–521. doi:10.1088/0034-4885/68/2/R06.

[56] X. Kou, X. Yao, J. Qiu, Negative permittivity and negative permeability of multi-walled carbon nanotubes/polypyrrole nanocomposites, Org. Electron. 38 (2016) 42–47. doi:10.1016/j.orgel.2016.07.029.

[57] P. Saini, V. Choudhary, B.P. Singh, R.B. Mathur, S.K. Dhawan, Enhanced microwave absorption behavior of polyaniline-CNT/polystyrene blend in 12.4-18.0 GHz range, Synth. Met. 161 (2011) 1522–1526. doi:10.1016/j.synthmet.2011.04.033.

[58] K. Lakshmi, H. John, K.T. Mathew, R. Joseph, K.E. George, Microwave absorption , reflection and EMI shielding of PU – PANI composite, Acta Mater. 57 (2009) 371–375. doi:10.1016/j.actamat.2008.09.018.

[59] K. Singh, A. Ohlan, R.K. Kotnala, A.K. Bakhshi, S.K. Dhawan, Dielectric and magnetic properties of conducting ferromagnetic composite of polyaniline with γ-Fe_2O_3 nanoparticles, Mater. Chem. Phys. 112 (2008) 651–658. doi:10.1016/j.matchemphys.2008.06.026.

[60] L. Yu, Y. Zhu, Y. Fu, Waxberry-like carbon@polyaniline microspheres with high-performance microwave absorption, Appl. Surf. Sci. 427 (2018) 451–457. doi:10.1016/j.apsusc.2017.08.078.

[61] J.C. Aphesteguy, A. Damiani, D. Digiovanni, S.E. Jacobo, Microwave absorption behavior of a polyaniline magnetic composite in the X-band, Phys. B Condens. Matter. 407 (2012) 3168–3171. doi:10.1016/j.physb.2011.12.055.

Figures, Tables and Captions

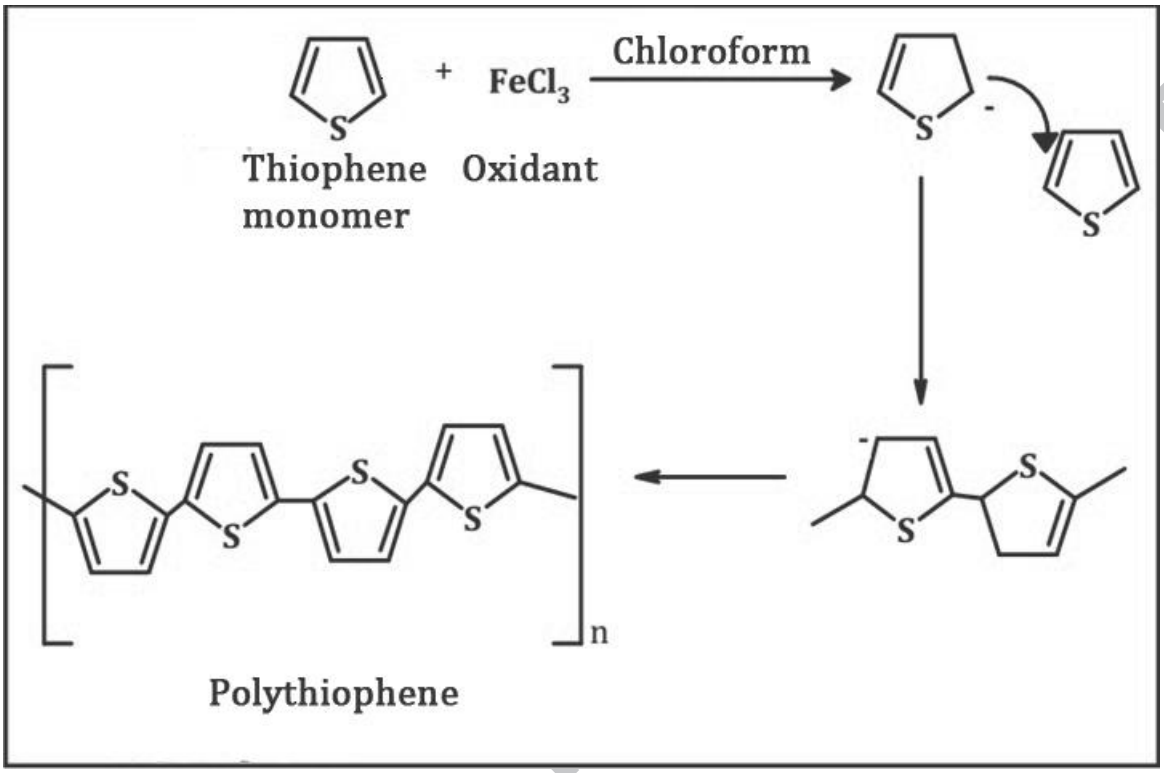

Fig.1. PTh thin film formation reaction mechanism

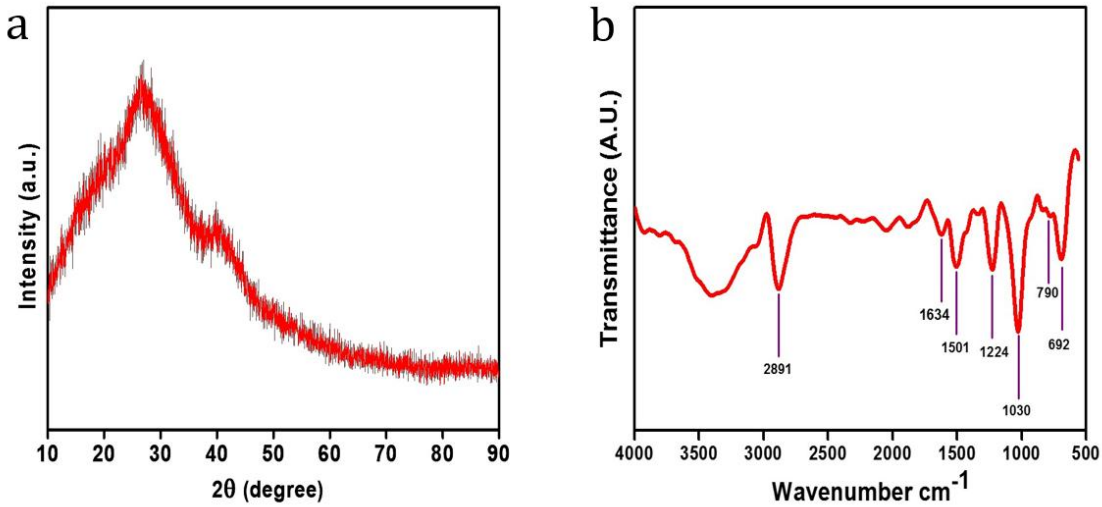

Fig. 2a. XRD pattern of pure PTh

Fig 2b. FTIR spectrum of pure PTh

FESEM and TEM study:

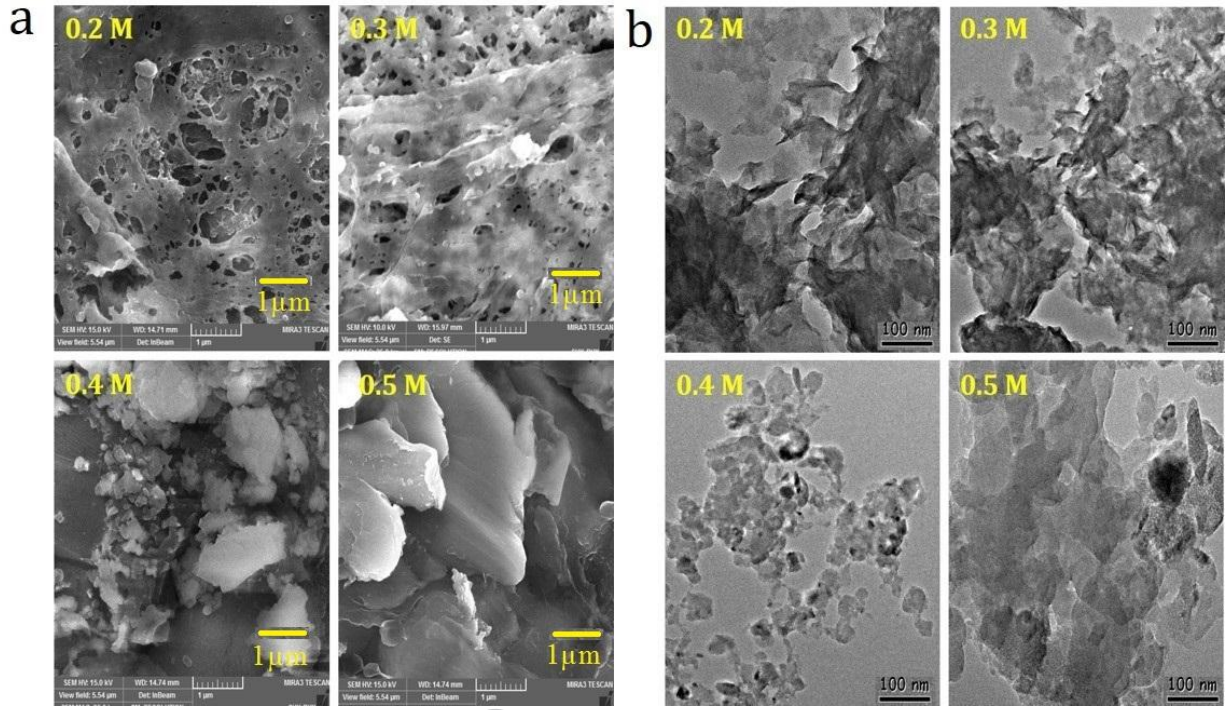

Fig. 3a. FESEM images of PTh thin films deposited at various monomer concentrations and

3b. TEM images of PTh thin films deposited at various monomer concentrations

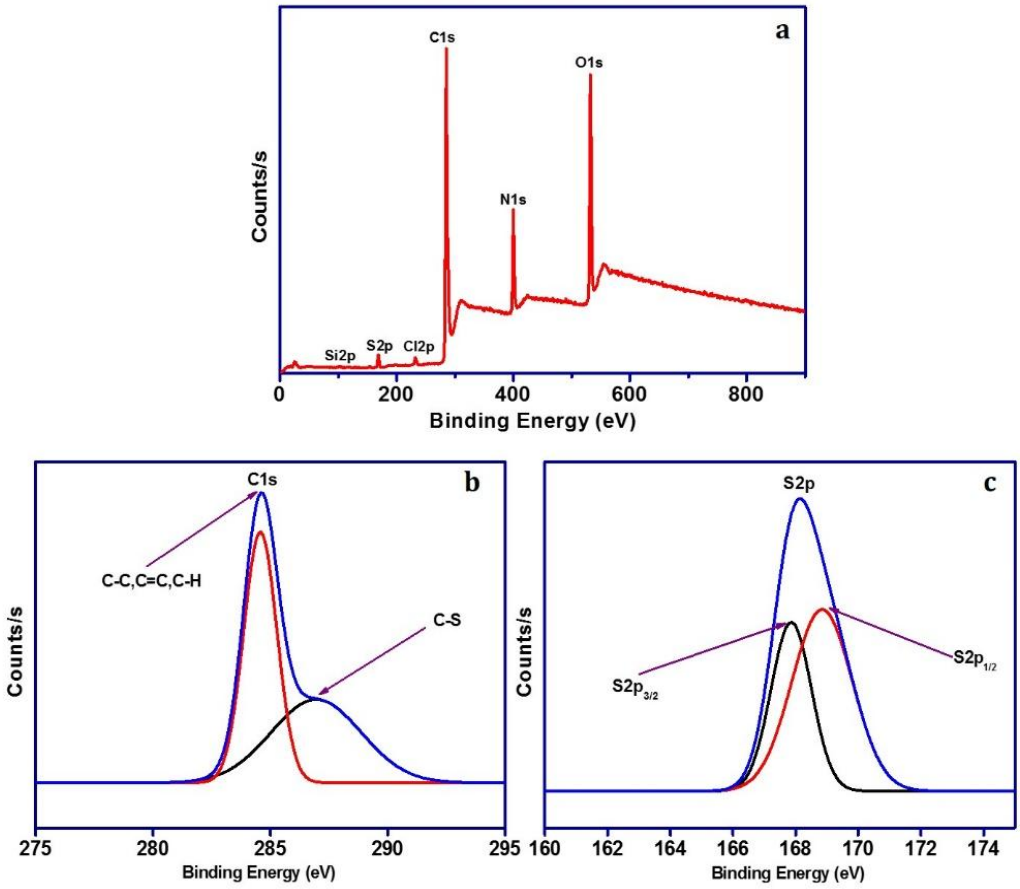

Fig. 4a. Survey scan XPS spectra of PTh, 4b. Narrow scan XPS spectra of C1s core level and 4c. Narrow scan XPS spectra of S2p core level

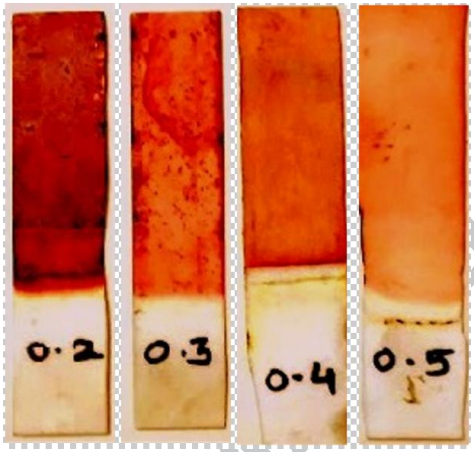

Fig.5. Thickness variation of PTh thin films deposited at various monomer concentrations

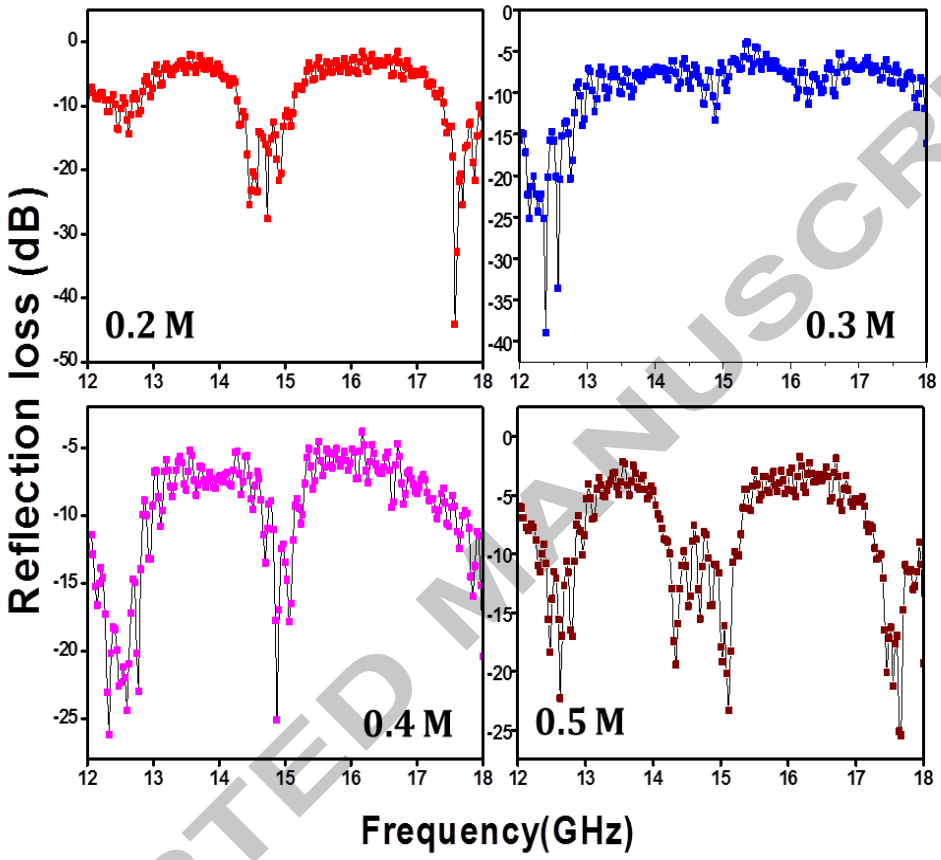

Fig.6. Reflection loss study of PTh thin films deposited at various monomer concentrations

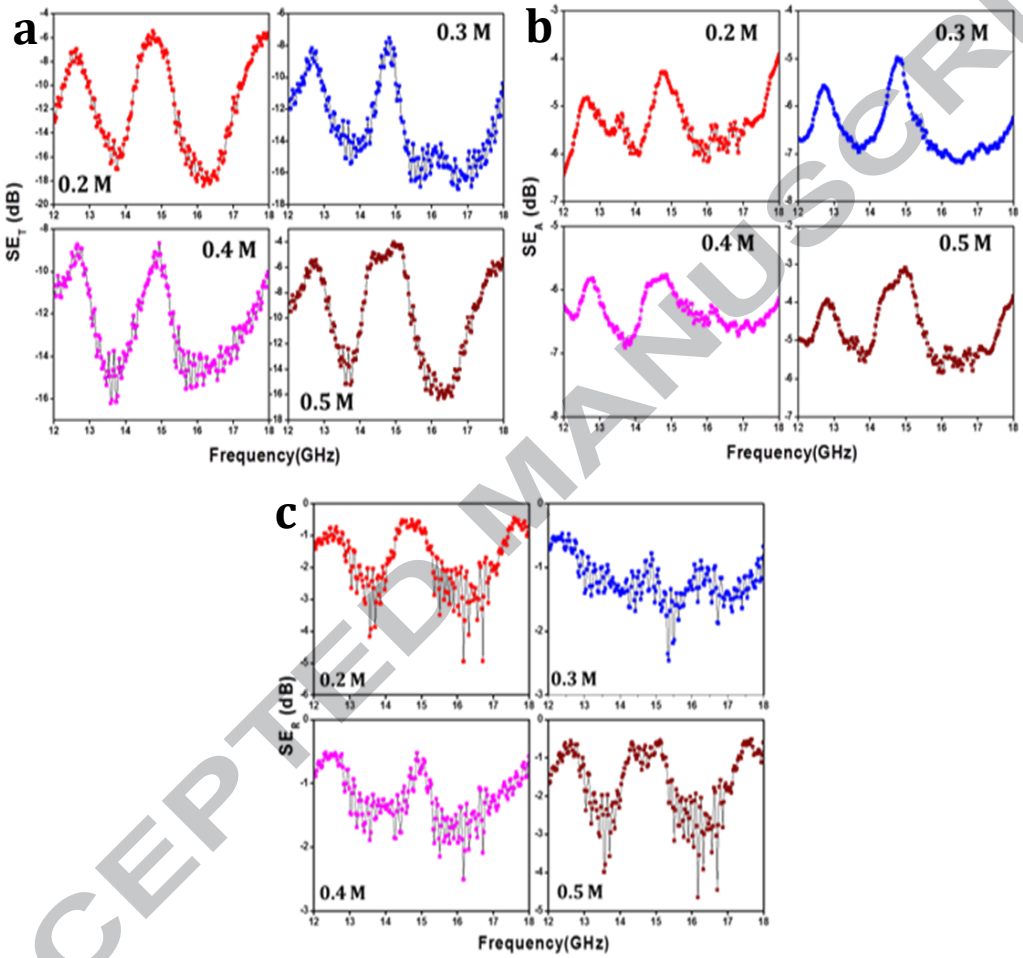

Fig.7a. Total shielding effectiveness of PTh thin films deposited at various monomer concentrations 7b. Shielding effectiveness due to absorption and 7c. Shielding effectiveness due to reflection

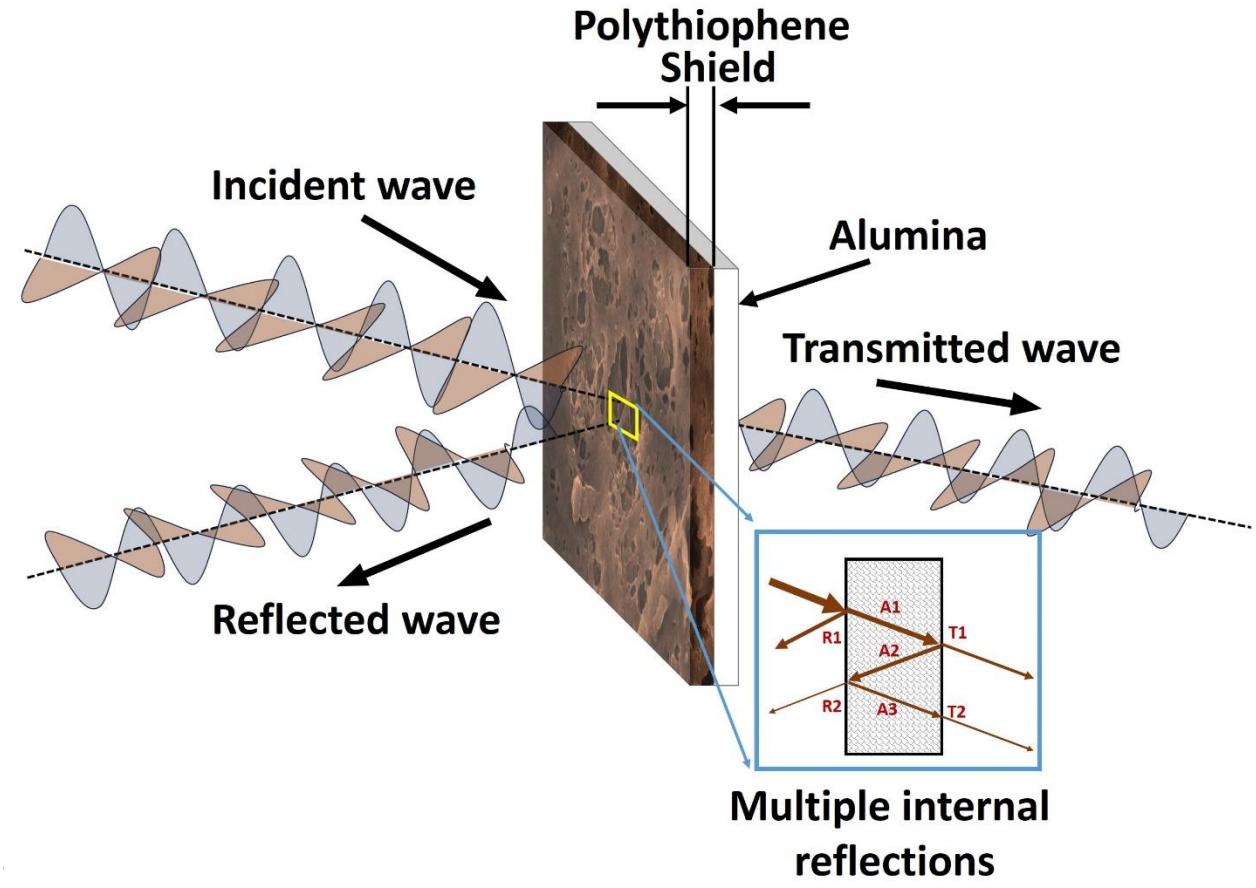

Fig. 8. Graphical representation of shielding mechanism

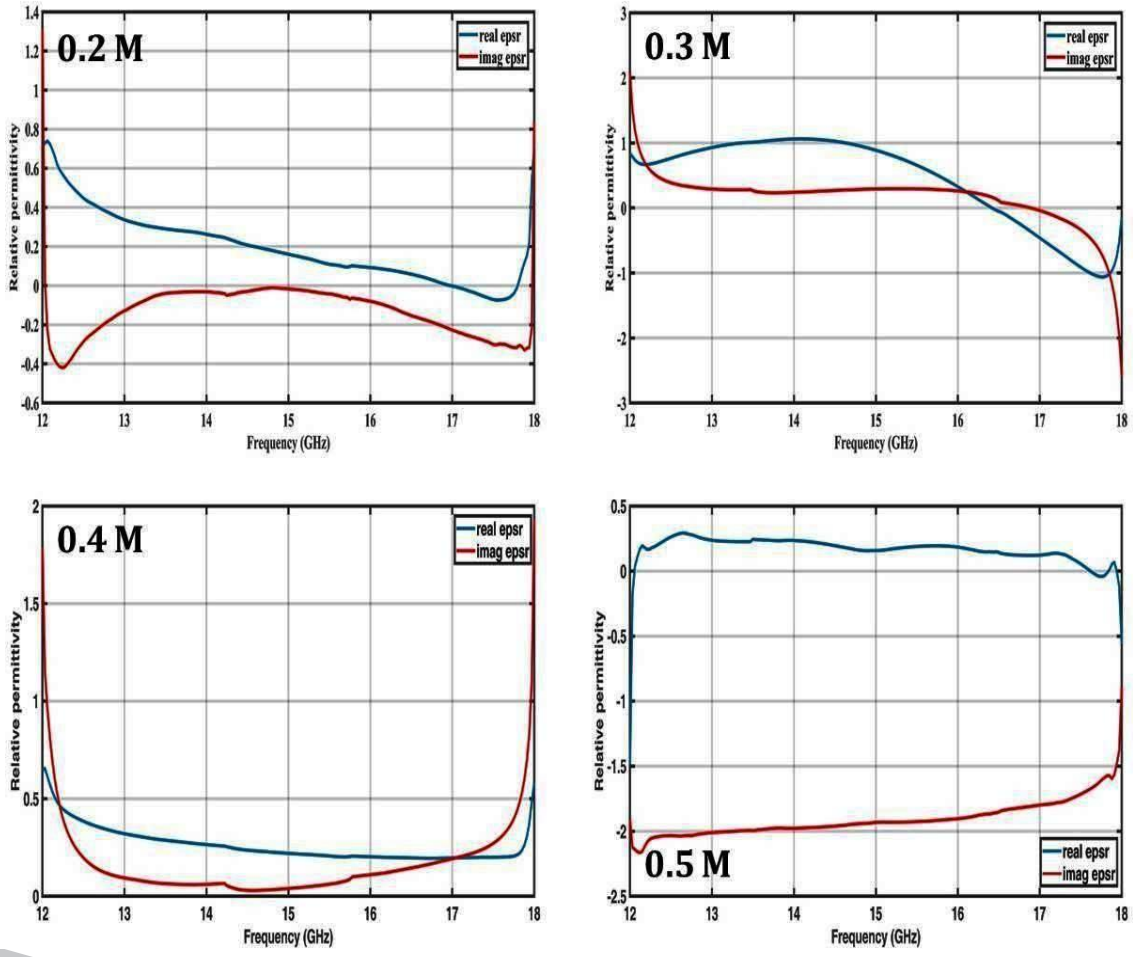

Fig. 9. Relative permittivity of PTh thin films deposited at various concentrations of thiophene

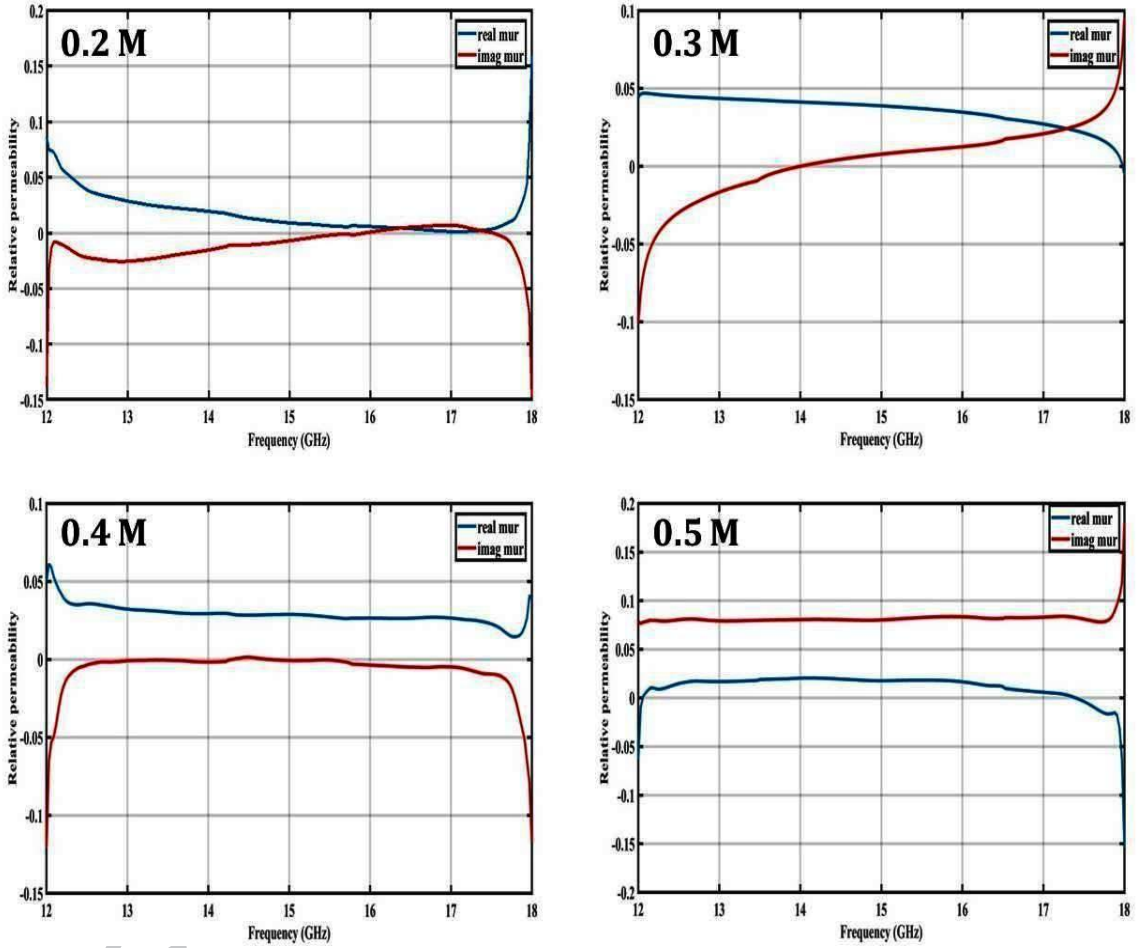

Fig.10. Relative permeability of PTh thin films deposited at various concentrations of thiophene

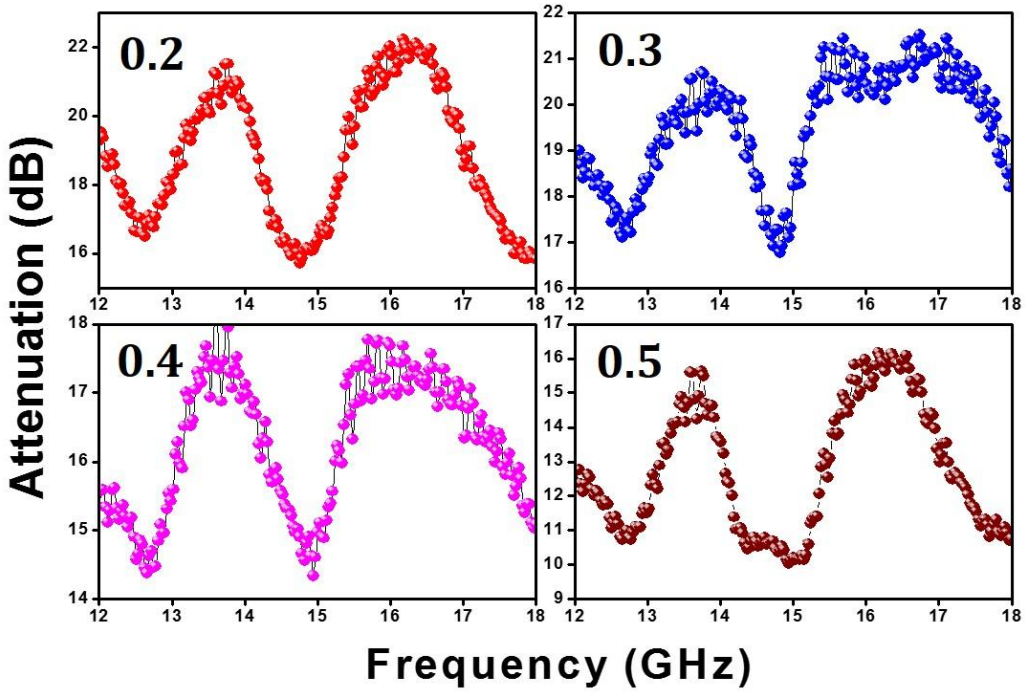

Fig.11. Microwave attenuation of PTh thin films deposited at various monomer concentrations

Sample	Oxidant	Conductivity (S/m)	Thickness (µm)
Pth (0.1 M)	*$FeCl_3$ (0.4 M)*	*-(No film formation)*	-
Pth (0.2 M)	*$FeCl_3$ (0.4 M)*	*5.412×10^{-3}*	*5.31*
Pth (0.3 M)	*$FeCl_3$ (0.4 M)*	*4.868×10^{-3}*	*4.56*
Pth (0.4 M)	*$FeCl_3$ (0.4 M)*	*4.126×10^{-3}*	*3.93*
Pth (0.5 M)	*$FeCl_3$ (0.4 M)*	*3.645×10^{-3}*	*3.37*

Table 1 Thickness and room temperature DC conductivity study of PTh thin films deposited at various monomer concentrations.

Sr.No.		RL(dB)	SE(dB)	Frequency (GHz)	Thickness	Ref.
1	PANI-MWCNT	NA	-45.7	12-18	2 mm	[57]
2	PANI/PU composite	-28.5	-26.7	8-12	1.9 mm	[58]
3	Polyaniline–$\gamma - Fe_2O_3$	NA	-11	8-12	NA	[59]
4	Carbon@PANI microspheres	-59.6	NA	2-18	2.2 mm	[60]
5	PANI-Fe_3O_4	NA	-4	8-12	1.5 mm	[61]
6	Fe_3O_4-PAA-PTh Composites	-13	NA	8-12	1.5 mm	[26]

7	*Polythiophene nanofibers*	*-8.5*	*NA*	*12-18*	*1.5 mm*	[26]
8	*Polyaniline nanofibers*	*NA*	*-13*	*8-18*	*50 micron*	[12]
9	*Polythiophene fibers*	*-44.41*	*-18.02*	*12-18*	*5.3 micron*	*This work*

Table 2 Comparison of RL and EMI SE of different polymer based materials in the 8-18 GHz frequency region

Exceptional electromagnetic interference shielding and microwave absorption properties of room temperature synthesized polythiophene thin films with double negative characteristics (DNG) in the Ku-band region

Gopal Kulkarni[1], Priyanka Kandesar[1], Ninad Velhal[1], Varsha Phadtare[1], Aviraj Jatratkar[1]**

S. K. Shinde[2], Dae-Young Kim[2], Vijaya Puri[1]*

[1]Thick and Thin Film Device laboratory, Department of Physics,

Shivaji University, Kolhapur - 416004, India

[2]Department of Biological and Environmental Science, College of Life Science and Biotechnology, Dongguk University-Ilsan, Biomedical Campus, Goyang-si, Gyeonggi-do, 410-773, Korea

Email: vrp_phy@unishivaji.ac.in*

Email: ninadvelhal@gmail.com**

GRAPHICAL ABSTRACT

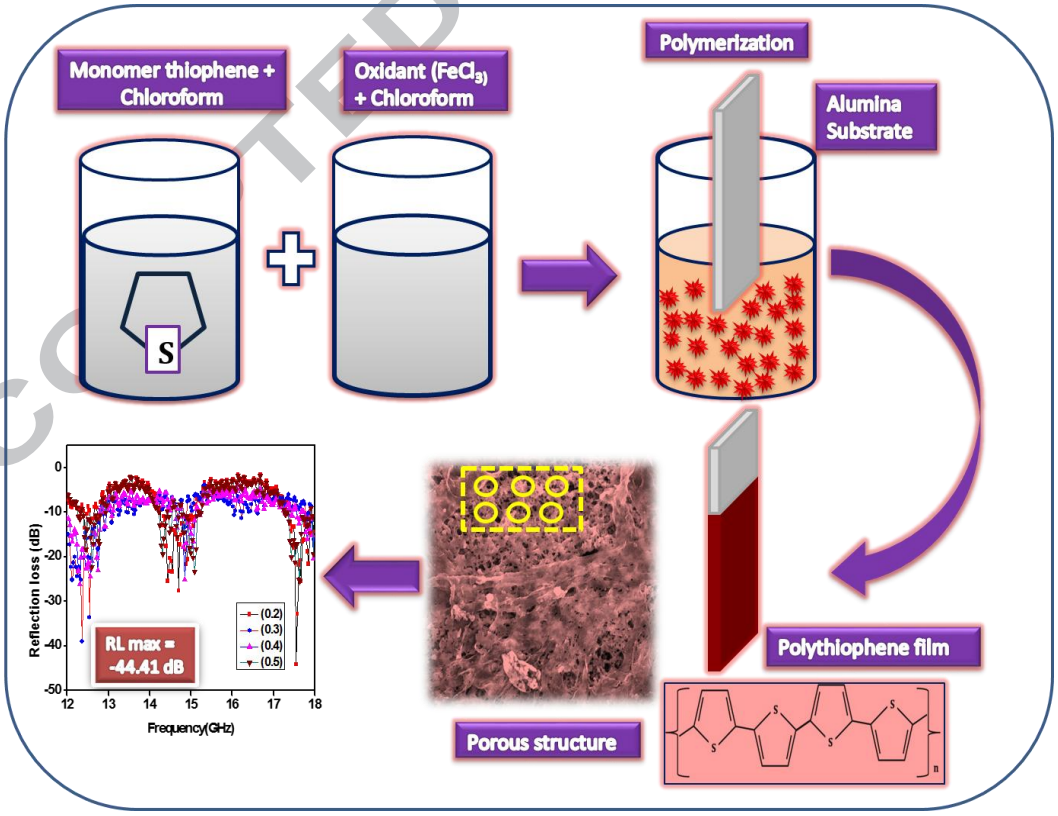

HIGHLIGHTS

- Facile synthesis of porous polythiophene (PTh) thin films at a room temperature
- The PTh thin films show DNG behavior in the Ku-band frequency region
- The PTh thin films exhibit exceptional shielding and microwave absorption performance
- The minimal reflection loss obtained for PTh thin film reaches -44.41 dB